Contribution from the Laboratoire de Chimie et Physico-Chimie Moléculaires, URA D0441 du CNRS, Ecole Centrale Paris, F-92295 Chatenay-Malabry Cedex, France, and Laboratoire de Chimie Quantique, UPR 139 du CNRS, Institut Le Bel, F-67000 Strasbourg, France

Tetracarbonylchloroethylidynechromium: Electron Deformation Density Revisited. Joint Multipole Model Refinement and ab Initio CASSCF Study

Anne Spasojevic-de Biré,[†,‡] Nguyen Quy Dao,[†] Alain Strich,[§] Claudine Thieffry,[§] and Marc Bénard*[,§]

Received October 25, 1989

The X-ray diffraction measurements obtained by Goddard and Krüger for $Cl(CO)_4Cr{\equiv}C{-}CH_3$ (crystallizing in $P2_1/c$; a = 6.504 (2) Å, b = 11.261 (5) Å, c = 12.756 (6) Å, β = 105.58 (3)°, Z = 4) have been refined by using the multipole model proposed by Hansen and Coppens. Static and dynamic model maps are obtained that provide suitable information concerning the reorganization of the electron density induced by the Cr≡C and Cr–$(CO)_4$ bonding. The observed alternation of the $Cr{-}C_{CO}$ bond lengths does not seem to be the consequence of a delocalized electronic effect originating in the methyl group. The static maps are discussed in connection with a theoretical density distribution obtained from ab initio CASSCF calculations. Both the theoretical and the multipole model maps show the marked covalent character of the Cr≡C π bonds, compared to the π back-donation occurring in the $Cr(CO)_4$ plane. The presence of a negative net charge on the carbynic carbon is confirmed, and the corresponding density accumulation is shown to lie in the region of the triple bond, facing the metal. This charge distribution is consistent with a $\sigma^2\pi^2$ formal electronic configuration for the carbynic carbon. The metal d-orbital populations deduced from the static model distribution are in quite good agreement with the theoretical predictions.

1. Introduction

An important and unexpected conclusion of previous theoretical studies on carbyne complexes[1-3] has been the evidence for a large negative net charge on the carbynic carbon atom. The consequences of this charge distribution in the interpretation of the nature and reactivity of the metal–carbon triple bond have been the subject of various discussions.[1-4] An X-ray determination of the density distribution of tetracarbonylchloroethylidynechromium, $Cl(CO)_4Cr{\equiv}C{-}CH_3$, has been reported some years ago by Goddard and Krüger (GK).[5] The X-X maps obtained by GK provided information of interest concerning the distribution of electron density around the metal and more specifically along the triple bond. The information unfortunately remained qualitative due to the effect of thermal smearing and the limitations of the spherical refinement. Multipole refinement techniques[6,7] now allow extraction of quantitative information from the diffraction measurements, more specifically concerning the metal orbital populations.[8] We therefore decided to apply Hansen and Coppens's multipole refinement[7] to the set of diffraction measurements obtained by GK and to compare the experimental model maps to a theoretical distribution obtained from ab initio CASSCF[9] calculations.

2. Experimental Deformation Density

2.1. Experimental Data. This compound, like all the members of the carbyne family, is very unstable, sensitive to moisture, to air, and to temperature. It decomposes slowly even at dry-ice temperature in sealed capillary tubes. Table I summarizes the X-ray diffraction experimental data for tetracarbonylchloroethylidynechromium (I) obtained by Krüger.[5] It is worthwhile noting that attempts to make single crystals of I for neutron diffraction studies have failed.

2.2. Multipolar Refinements. The refinements were carried out according to the Hansen–Coppens[7] model, using program MOLLY. In this model, the crystal is defined as a superposition of nonspherical pseudoatoms whose electronic density is described by an expansion of atom-centered deformation functions:

$$\rho_k(\vec{r}) = P_{kc}\rho_{k,\mathrm{core}}(\vec{r}) + P_{kv}\kappa_k^3\rho_{k,\mathrm{valence}}(\kappa_k r) + \sum_{l=0}^{4}\kappa'^3_k R_{k,l}(\kappa'_k r)\sum_{m=-1}^{+1} P_{k,lm}Y_{lm}(\vec{r}/r) \quad (1)$$

where ρ_{core} and ρ_{valence} are spherical Hartree–Fock core and valence densities, Y_{lm} represent the spherical harmonic angular function in real form, κ and κ' are expansion–contraction parameters, and R_{lm} represent the Slater-type radial functions defined as

$$R_{lm} = Nr^n n_l e^{-\kappa'\zeta_l r} \quad (2)$$

where n_l and ζ_l depend on the nature of the atom and its chemical environment and P_{lm} is the multipole population coefficient.[7]

Table I. Crystallographic Data for $Cl(CO)_4Cr{\equiv}C(CH_3)$ (I)

cell data	
a, Å	6.504 (2)
b, Å	11.261 (5)
c, Å	12.756 (6)
α, deg	90.0
β, deg	105.58 (3)
γ, deg	90.0
V, Å^3	899.96
Z	4
d_c, g cm^{-3}	1.67
space group	$P2_1/c$
T, K	100
radiation, (λ, Å)	Mo Kα, Zr filter (0.71069)
no. of reflections	
tot.	4742
independent	2372
$F > 2\sigma$	1836
μ, cm^{-1}	15.2

Table II. Initial Radial Functions[a]

	l = 1		2		3		4	
	n_l	$\zeta_l\kappa'$	n_l	$\zeta_l\kappa'$	n_l	$\zeta_l\kappa'$	n_l	$\zeta_l\kappa'$
Cr	4	6.40	4	6.40	4	6.40	4	6.40
Cl	4	5.50	4	5.50	4	5.50	4	5.50
C	2	3.20	2	3.20	3	3.20	4	3.20
O	2	3.40	2	3.40	3	3.40	4	3.40
H	2	1.30						

[a] $\zeta_l\kappa'$ in Å^{-1}.

Table III. Scattering Form Factors[a]

	core electrons			core electrons		
	sf	ne	ref	sf	ne	ref
Cr	$f(Cr^{3+})_{Ar\ core}$	18	11	$f(Cr)_{free} - f(Cr^{3+})_{Ar\ core}$	6	11
Cl	$f(Cl)_{Ne\ core}$	10	11	$^1/_7(2\langle j0\rangle_{3s} + 5\langle j0\rangle_{2p})$	7	11
C	$f(C)_{Ne\ core}$	2	11	$^1/_2(\langle j0\rangle_{2s} + \langle j0\rangle_{2p})$	4	11
O	$f(O)_{Ne\ core}$	2	11	$^1/_3(\langle j0\rangle_{2s} + 2\langle j0\rangle_{2p})$	6	11
H		0		Stewart et al.	1	12

[a] Anomalous scattering form factors are defined for the chromium and chloride atoms.[11] sf = scattering form factor; ne = number of electrons attributed to this part.

[†] Ecole Centrale Paris.

[‡] Present address: Laboratoire Léon Brillouin, CEA-CNRS, CEN Saclay, F-91191 Gif-sur-Yvette Cédex, France.

[§] Laboratoire de Chimie Quantique.

(1) (a) Kostic, N. M.; Fenske, R. F. *J. Am. Chem. Soc.* **1981**, *103*, 4677. (b) Kostic, N. M.; Fenske, R. F. *Organometallics* **1982**, *1*, 489.
(2) Ushio, J.; Nakatsuji, H.; Yonezawa, T. *J. Am. Chem. Soc.* **1984**, *106*, 5892.

0020-1669/90/1329-4908$02.50/0

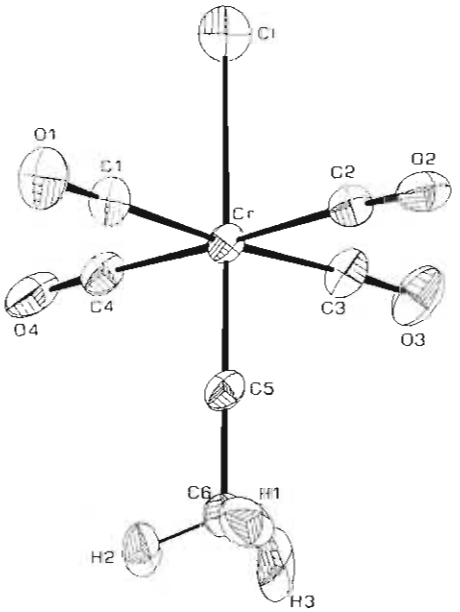

Figure 1. Molecular geometry of I (ORTEP diagram with multipolar parameters).

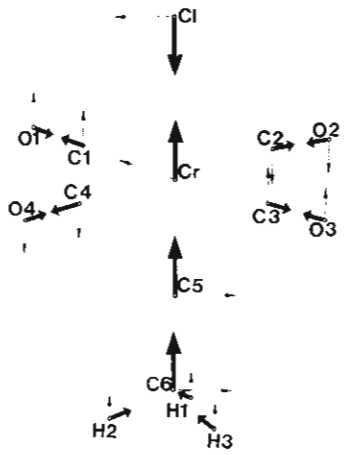

Figure 2. Local Cartesian axis systems defined for each atom in the multipolar refinement. The bold arrow defines the z axis, and the second arrow, the x axis, except for the C6 atom, where it is the y axis. The third axis is choosen so as to define a direct orthogonal system.

Table IV. Reliability Factors[a]

method	$R(F)$, %	$R_w(F)$, %	$R(F^2)$, %	$R_w(F^2)$, %	GOF	NO[b]	NV[c]
1[d]	2.64	2.95	3.56	6.22	1.78	1836	109
2[d]	3.01	2.69	4.16	5.26	1.09	773	109
3[d]	3.14	2.82	4.37	5.53	1.09	773	37
4[d]	2.07	2.24	2.86	4.94	1.37	1836	161
5[d]	2.08	2.26	2.87	4.95	1.36	1836	91

[a] $R(F) = \sum_{all}|F_o - k|F_c||/\sum_{all}F_o$. $R_w(F) = [\sum_{all}w|F_o - k|Fc||^2/\sum_{all}w'F_o^2]^{1/2}$ ($w = 1/\sigma^2(F_o^2)$). $R(F^2) = \sum_{all}|F_o - (k|F_c|^2|/\sum_{all}F_o^2$. $R_w(F^2) = [\sum_{all}w|F_o - (k|F_c| - (k|F_c|)^2|^2/\sum_{all}wF_o^4]^{1/2}$ ($w' = 1/\sigma^2(F_o)$). GOF = $[\sum_{all}w|F_o - k|F_c||^2/(NO - NV)]^{1/2}$. [b] NO = number of independent observed reflections. [c] NV = number of variables. [d] Methods key: (1) spherical refinement; (2) high-order refinement isotropic temperature factors for hydrogen atoms; (3) high-order refinement anisotropic temperature factors for hydrogen atoms; (4) multipolar refinement step i; (5) multipolar refinement step ii. Refinements are based on F. In refinement methods 1 and 4, we keep fixed the parameters of the hydrogen atoms at the value obtained in method 2. In refinement method 5, we keep fixed the parameters of the hydrogen atoms at the value obtained in method 3.

Table II represents the values of n_l and $\kappa'\zeta_l$ defining the initial radial functions of the different types of atoms, while Table III gives the chosen

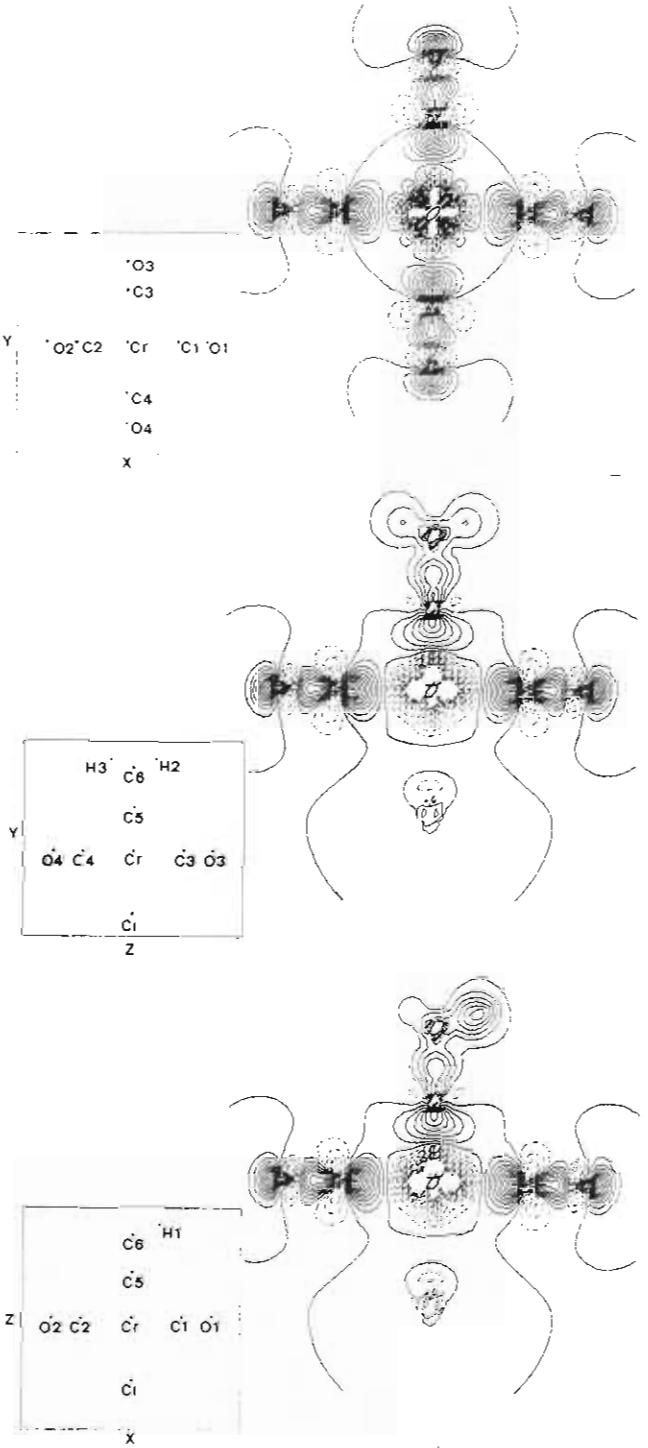

Figure 3. Theoretical deformation density maps, showing the difference between the density obtained from the CASSCF wave function of I and the density generated by a superposition of spherically averaged atoms computed with the same basis sets: (a, top) $Cr(CO)_4$ plane; (b, middle, and c, bottom) perpendicular planes containing the Cl—Cr≡C—C axis. Contour intervals are 0.1 e Å^{-3}. Negative contours are dashed.

atomic scattering factors of different atoms of I, according to refs 12 and 13. In order to keep the number of the P_{lm} parameters at a minimum

(3) Poblet, J. M.; Strich, A.; Wiest, R.; Bénard, M. *Chem. Phys. Lett.* **1986**, *126*, 169.

(4) (a) Nguyen Quy Dao; Spasojevic-de Biré, A.; Fischer, E. O.; Becker, P. J. *C. R. Acad. Sci. Paris* **1988**, *307II*, 341. (b) Nguyen Quy Dao; Neugebauer, D.; Février, H.; Fischer, E. O.; Becker, P. J.; Pannetier, J. *Nouv. J. Chim.* **1983**, *6*, 359.

(5) Goddard, R.; Krüger, C. In *Electron Distributions and the Chemical Bond*; Coppens, P., Hall, M. B., Eds.; Plenum Press: New York, 1982; pp 297–330. (b) Krüger, C.; Goddard, R.; Claus, K. H. *Z. Naturforsch.* **1983**, *38B*, 1431.

(6) Hirshfeld, F. L. *Isr. J. Chem.* **1977**, *16*, 226.

(7) Hansen, N. K.; Coppens, P. *Acta Crystallogr., Sect. A* **1978**, *A34*, 909.

Table V. Atomic Positional Parameters (Å × 10^5)

	refinement method[a]	x	y	z
Cr	1	26977 (5)	17326 (3)	24800 (2)
	2	26984 (7)	17325 (5)	24803 (4)
	5	26976 (4)	17327 (4)	24799 (3)
Cl	1	34635 (8)	32889 (5)	13076 (4)
	2	34639 (10)	32987 (8)	13071 (6)
	5	34639 (6)	32899 (5)	13071 (4)
O1	1	73571 (24)	19435 (14)	37771 (13)
	2	73648 (51)	19358 (27)	37784 (27)
	5	73720 (51)	19420 (11)	37821 (17)
O2	1	12668 (26)	36632 (13)	38870 (14)
	2	12670 (55)	36679 (29)	38858 (32)
	5	12601 (26)	36711 (22)	38920 (18)
O3	1	−18812 (24)	15329 (13)	10760 (13)
	2	−18962 (12)	15378 (26)	10724 (33)
	5	−18968 (51)	15331 (11)	10709 (17)
O4	1	40598 (25)	−1903 (13)	10503 (13)
	2	40691 (52)	−1925 (28)	10458 (23)
	5	40660 (24)	−1976 (23)	10448 (17)
C1	1	56343 (34)	18842 (17)	33004 (16)
	2	56375 (51)	18835 (24)	33013 (25)
	5	56408 (50)	18826 (14)	33029 (18)
C2	1	18243 (32)	29699 (17)	33898 (17)
	2	18036 (49)	29770 (26)	33701 (27)
	5	18226 (29)	29728 (22)	33706 (20)
C3	1	−1896 (33)	16353 (16)	15736 (17)
	2	−1919 (52)	16323 (25)	15683 (27)
	5	−1938 (49)	16355 (13)	15716 (18)
C4	1	35809 (33)	5415 (18)	15489 (17)
	2	35840 (48)	5391 (27)	15484 (27)
	5	35800 (29)	5396 (23)	15472 (18)
C5	1	22021 (30)	6533 (16)	33145 (16)
	2	22037 (42)	6500 (22)	33215 (24)
	5	21987 (41)	6438 (25)	33223 (23)
C6	1	18154 (32)	−2785 (16)	40380 (17)
	3	18111 (50)	−2859 (23)	40439 (26)
	5	18099 (50)	−2822 (24)	40424 (23)
H1	1	21096 (310)	437 (170)	48020 (160)
	3	21270 (723)	284 (281)	48217 (276)
	5	21270 (723)	284 (281)	48217 (276)
H2	1	28300 (330)	−9295 (190)	40408 (170)
	3	26774 (816)	−9146 (315)	40478 (278)
	5	26774 (816)	−9146 (315)	40478 (278)
H3	1	3241 (390)	−5323 (190)	38204 (180)
	3	2078 (899)	−4881 (299)	38387 (282)
	5	2078 (899)	−4881 (299)	38387 (282)

[a] Defined in Table IV.

while respecting the chemical environment of each atom, we define for the atoms local symmetries that are the following: for Cr and Cl, C_{4v}; for the CO groups, C_{2v}; for C5, C6, and H3, C_s; for H1 and H2, no symmetry. Because of convergence problems, it was not possible to refine the κ' coefficients as usually done in the Hansen–Coppens model.[7] The expansion–contraction coefficients were kept fixed at the values given in Table VI. Figure 1 shows the molecular structure of I, and Figure 2, the local Cartesian axes.

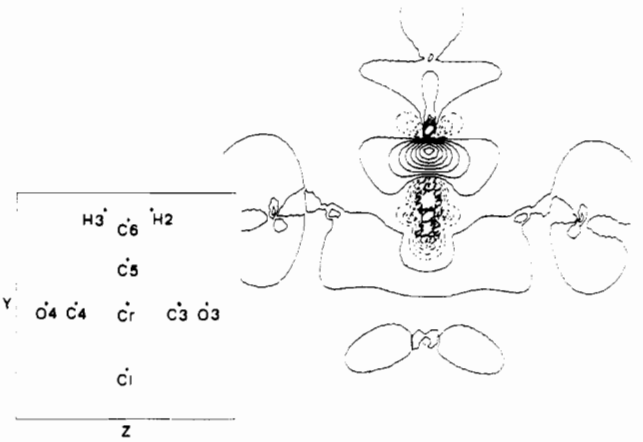

Figure 4. Theoretical deformation density map with respect to the superposition of the $ClCr(CO)_4$ and CCH_3 fragments both computed in their quartet $\sigma^1\pi^2$ states. The map shows the plane containing the Cl—Cr≡C—C axis (same as in Figure 3b). Contour intervals are as in Figure 3.

Table VI. Multipole Parameters[a]

	Cr	Cl	O1–O4	C1–C4
κ	0.872 (19)	0.965 (8)	0.971 (4)	0.991 (7)
κ'	0.800	1.000	1.000	0.800
P_v	5.594 (136)	7.427 (81)	6.462 (26)	3.520 (270)
P_{10}	0.005 (39)	0.069 (26)	0.366 (146)	−0.298 (135)
P_{20}	0.004 (64)	0.050 (40)	0.345	0.183 (105)
P_{22+}	0.000	0.000	−0.023 (43)	0.022 (32)
P_{30}	−0.063 (32)	0.049 (30)	0.187 (72)	−0.037 (64)
P_{32+}	0.000	0.000	−0.041 (33)	0.040 (30)
P_{40}	−0.203 (50)	−0.400 (47)	0.071 (49)	−0.109 (46)
P_{42+}	0.000	0.000	−0.013 (35)	0.007 (31)
P_{44+}	0.266 (41)	−0.016 (49)	−0.017 (25)	−0.003 (21)
	C5	C6	H1, H2	H3
κ	0.988 (21)	0.915 (17)	1.000	1.000
κ'	0.800	0.800	1.000	1.000
P_v	3.883 (223)	5.100 (307)	0.699 (57)	0.665 (72)
P_{11+}	−0.009 (43)	−0.114 (92)	0.111 (53)	−0.157 (104)
P_{11-}	0.000	0.037 (56)	0.026 (56)	0.000
P_{10}	0.405 (96)	0.000	0.004 (80)	0.048 (115)
P_{20}	0.187 (115)	−0.180 (64)		
P_{21+}	−0.042 (57)	0.000		
P_{22+}	−0.055 (40)	0.137 (83)		
P_{22-}	0.000	0.015 (63)		
P_{30}	−0.057 (62)	0.000		
P_{31+}	−0.040 (45)	0.189 (57)		
P_{31-}	0.000	−0.162 (49)		
P_{32+}	0.049 (36)	0.000		
P_{33+}	0.000	−0.300 (63)		
P_{33-}	−0.025 (29)	0.034 (46)		
P_{40}	−0.087 (80)	0.143 (50)		
P_{41+}	0.013 (39)	0.000		
P_{42+}	−0.013 (47)	−0.158 (51)		
P_{42-}	0.000	0.015 (53)		
P_{43+}	0.080 (43)	0.000		
P_{44+}	0.008 (36)	0.055 (51)		
P_{44-}	0.000	−0.025 (52)		

[a] The parameters are those obtained after the refinement method 5. We have used some constraints and have also refined one carbonyl group, so all the parameters of C1–C4 (O1–O4, respectively) are equal. The hydrogen atoms H1 and H2 are also constrained. The κ' expansion–contraction coefficient was not refined because it quickly diverges.

Finally, in order to compare the results obtained by multipolar models with those of the spherical model refinement, we used the same scattering factors in both models.

Due to the fact that the number of observed reflections is small compared to the total number of parameters in the multipolar model, we defined a two-step refinement strategy: (i) All the atoms are refined in their ideal symmetry, i.e. C_{4v} for Cr, Cl, C5, and C6 and C_{2v} for CO, H1,

(8) Holladay, A.; Leung, P.; Coppens, P. *Acta Crystallogr., Sect. A* **1983**, *A39*, 377.
(9) (a) Roos, B. O.; Taylor, P. R.; Siegbahn, P. E. M.. *Chem. Phys.* **1980**, *48*, 157. (b) Siegbahn, P. E. M.; Almlöf, J.; Heiberg, A.; Roos, B. O. *J. Chem. Phys.* **1981**, *74*, 2384. (c) Roos, B. O. *Int. J. Quantum Chem.* **1980**, *S14*, 175.
(10) Pitzer, R. M. *J. Chem. Phys.* **1973**, *58*, 3111.
(11) Nguyen Quy Dao; Foulet-Fonseca, G. P.; Jouan, M.; Fischer, E. O.; Fischer, H.; Schmid, J. *C. R. Acad. Sci. Paris* **1988**, *307II*, 245.
(12) *International Tables for X-ray Crystallography*; Kynoch, Press: Birmingham, England, 1974; Vol. IV, pp 103–118.
(13) Stewart, R. F.; Davidson, E. R.; Simpson, W. T. *J. Chem. Phys.* **1965**, *42*, 3175.

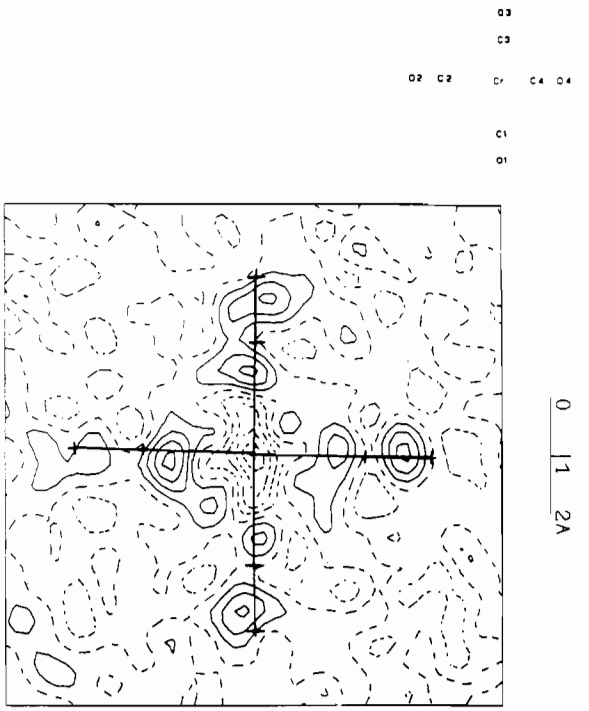

Figure 5. X–X spherical density map, as defined from eq 3, in the average $Cr(CO)_4$ plane. Contour intervals are 0.1 e Å^{-3}. Zero and negative contours are dashed. The phase of the observed structure factor F_1 is obtained by using a *spherical* model for the bonded molecule. The computed structure factor F_2 is obtained by using a free atom model with parameters deduced from a *high-order* refinement.

H2, and H3. (ii) Once the refinement defined in step i has converged, the atoms C5, C6, H1, H2, and H3 are considered in their real symmetry defined above by keeping all the parameters of the CO groups fixed as obtained in step i.

Table IV gives the different reliability factors of these refinements, and Tables V and VI give the multipolar parameters as obtained in the last cycles.

2.3. Electron Density Map. The electron deformation densities are calculated as follows:

$$\rho_{def}(\vec{r}) = \frac{1}{V}\sum\left(\frac{F_1}{k} - F_2\right)e^{-2i\pi\vec{H}\vec{r}} \qquad (3)$$

where k is the scale factor, and F_1 and F_2, depending on the map type, are defined in the figure captions. For the X–X maps, the computed structure factor F_2 is obtained by using a free atom model with parameters deduced from a high-order refinement (Figure 5). Differences in the computation of F_2 should explain the modifications of the present X–X maps (Figure 5) with respect to those of Goddard and Krüger.[5] In the experimental and dynamical multipolar deformation density maps, the κ values have been obtained by multipolar refinement in the free atom model, instead of simply taking $\kappa = 1$ as normally done (we observed that in fact there is a slight improvement when using the refined κ value). Figure 5 shows the experimental X–X maps in the average plane of the four carbonyls. Figure 6 displays the X–M maps in the same plane (Figure 6a) and in the plane containing the metal–carbyne axis and one C–H bond (Figure 6b). The residual series of the two models are provided as supplementary material. A comparison of the two series of refinements leads to the following comments:

(i) Concerning the interatomic distances, the multipolar results differ slightly from high-order results. However, the results obtained by using the multipolar model seem of better quality, since they give more consistent data. A similar remark can be made concerning the Cr≡C5 distance, 1.718 (3) Å from the multipolar model and 1.711 (3) Å from high-order refinement. For the phenylcarbyne complex (II)[4] (where the methyl group is replaced by a phenyl group), $d_{Cr\equiv C}$ = 1.723 (1) Å from multipolar refinement, 1.716 (1) Å from high-order refinement, and 1.725 (4) Å from neutron diffraction. Concerning the C–H bonds of the methyl group, the obtained lengths are not really meaningful, as will be discussed in part iv.

(ii) In the deformation density maps, the density distribution along the Cr–C4 and Cr–C2 bonds, on the one hand, and the Cr–C1 and Cr–C3 bonds, on the other hand, should be similar, since the metal–carbon distances are identical two by two. As a matter of fact, as displayed on the experimental spherical deformation maps (Figure 5), the density peak associated with the Cr–C2 bond is much higher than that of the Cr–C4 bond. Conversely, the C≡O deformation density obtained from spherical refinement is not symmetrical either: the peaks associated with the C3–O3 and the C4–O4 bonds are stronger than those corresponding to the C1–O1 and C2–O2 bonds. One can also notice that the accumulation associated with Cr–C2 is higher than the one of C2–O2, at variance from what is obtained for the three other metal–carbonyl bonds (Figure 5). Much better results are obtained with the X–M multipolar density maps, and the deformation density map in the $Cr(C-O)_4$ plane no longer leads to contradictions (Figure 6).

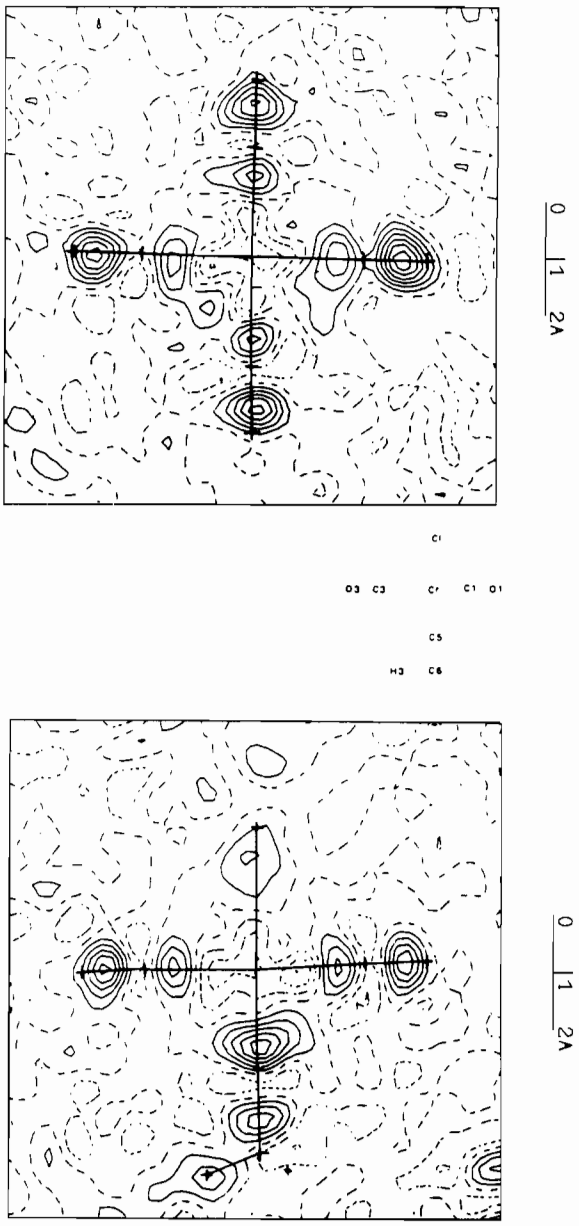

Figure 6. X–M multipolar density maps: (a, top) average $Cr(CO)_4$ plane; (b, bottom) plane containing Cr, Cl, and O1 (distance from the plane to atoms C1, C3, O3, C5, C6, and H3 less than 0.1 Å). Contours are defined as in Figure 5. The phase of the observed structure factor F_1 is obtained by using a *multipolar* model for the bonded molecule. The computed structure factor F_2 is obtained by using a free atom model with parameters deduced from a *multipolar* refinement.

(iii) The better quality of the multipolar refinement can also be noticed from a comparison of the residual series of the two refinements. Residual density (considered here as a noise) is still quite high in the spherical model (Figure 5), especially in the region of the $Cr\equiv C_{carbyne}$ triple bond and in the direction of the d_{xy} orbitals of the Cr atom. Once the multipolar models are considered, the residual peaks are noticeably reduced and the noise is more regularly distributed.

(iv) In a discussion concerning the symmetry of the methylcarbyne molecule, Krüger[5] suggested that I exists in an eclipsed configuration, the C–H3 bond being practically coplanar to C≡Cr—C3≡O3. In a

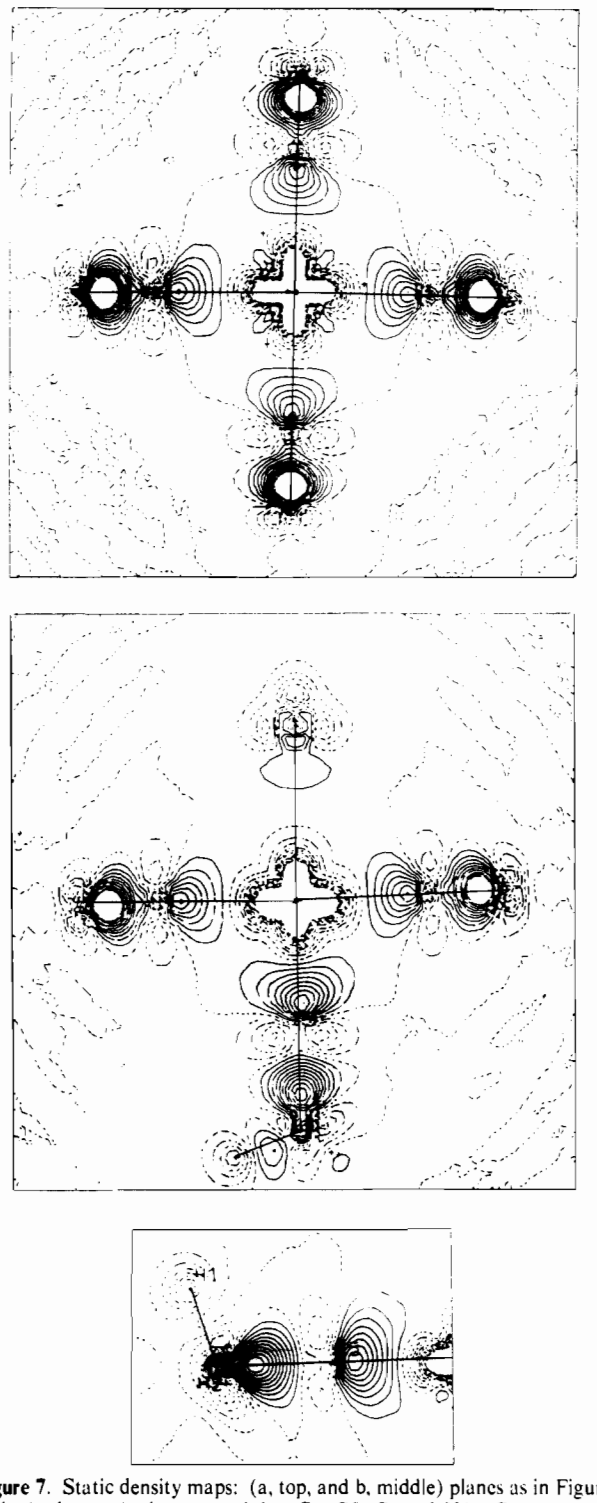

Figure 7. Static density maps: (a, top, and b, middle) planes as in Figure 6a,b; (c, bottom) plane containing Cr, C5, C, and H1. Contours are defined as in Figure 5.

previous work dedicated to the spectroscopic investigation of hyperconjugation in I, one of us (N.Q.D.) has shown[11] that I is in fact a mixture of two conformers, an eclipsed conformer (E) and a noneclipsed one (NE) (Figure 9), the proportion of the two forms depending on the temperature. At 77 K, only the E conformer exists, but at 100 K, 33% of NE is already present. The positions of the protons were determined with sufficient accuracy to establish that the dihedral angle between C–H3 and Cr—C3≡O3 is not zero but approximately 8°, which is the weighted average value between the E and the NE positions (Table S3, supplementary material). This observation seems to confirm the results obtained by spectroscopy and also partly explains the difficulty to clearly observe the electronic density along the C–H bonds.

(v) Figures 7a,b and 8a,b, respectively, display the static and the dynamic density maps of I. The metal d-orbital populations, as derived from the multipolar model,[8] are summed up in Table VII and compared

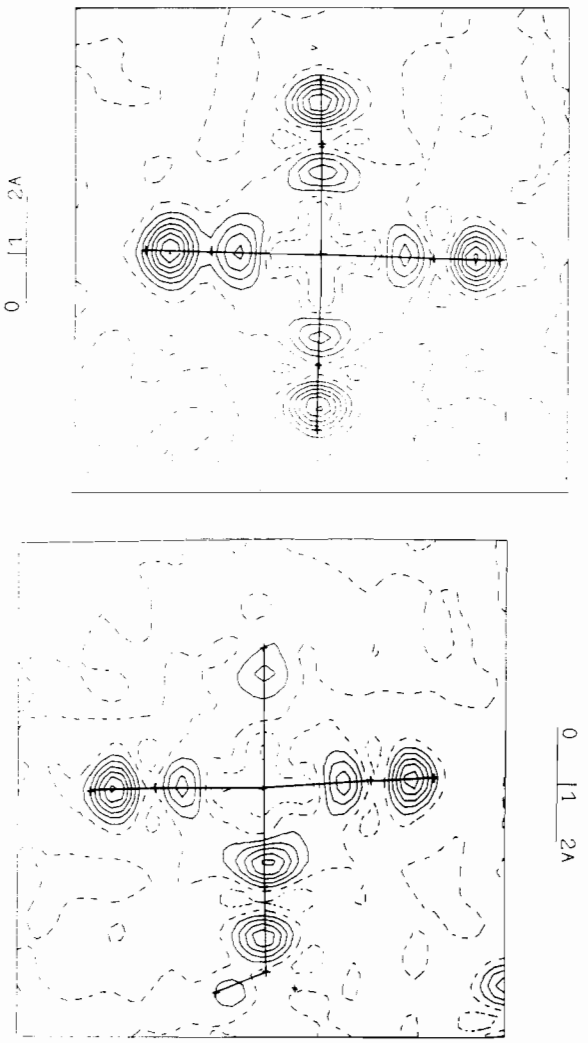

Figure 8. X–M dynamic density maps. Maps, planes, and contours are defined as in Fi[illegible] a,b. The structure factors F_1 and F_2 are defined as in Figure 6.

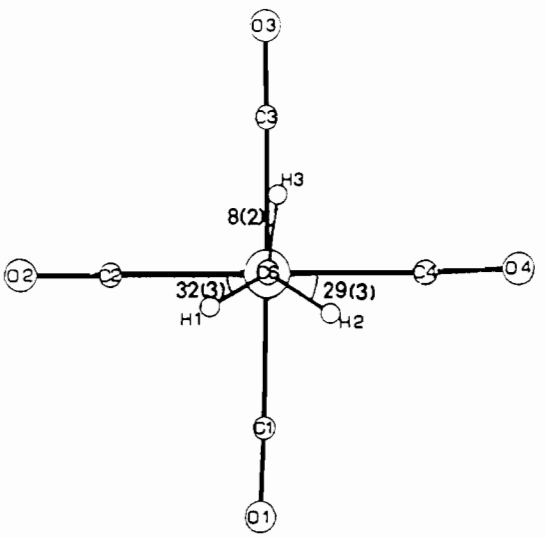

Figure 9. Dihedral angles of the methyl group.

to the populations obtained from the Mulliken analysis of the ab initio CASSCF wave function.

3. Computational Details

Ab initio calculations have been carried out at the CASSCF[9] level with the ARGOS program system[10] for the calculation of molecular integrals, and the program written by Siegbahn et al.[9b] was used for CASSCF iterations. The observed geometrical parameters have been

Table VII. Populations (e) of the Metal d Orbitals, from the Multipole Refinements and the ab Initio CASSCF Calculations, and Net Atomic Charges (e), from ab Initio Calculations

	$Cl(CO)_4Cr{\equiv}CCH_3$ multipolar ref		$Cl(CO)_4Cr{\equiv}CCH_3$ ab initio (CASSCF/6)[a]		$Cl(CO)_4Cr{\equiv}CH$		
						CASSCF/8[b]	
	popln	%	popln	%	CASSCF/6 popln	popln	%
d_{z^2}	0.8 (4)	15	0.73	14	0.78	0.75	15
$d_{xz} + d_{yz}$	2.6 (4)	47	2.28	44	2.24	2.31	45
$d_{x^2-y^2}$	0.6 (4)	12	0.43	8	0.44	0.51	10
d_{xy}	1.5 (4)	27	1.72	33	1.74	1.59	31
tot.	5.60 (8)		5.16		5.20	5.16	
Cr			+0.33		+0.28	+0.29	
C_{CO}			+0.23		+0.22	+0.22	
O			−0.37		−0.36	−0.36	
$C_{Cr{\equiv}C}$			−0.32		−0.39	−0.36	
C_{Me}			−0.45				
H_{Me}			+0.17				
H_{CH}					+0.16	+0.17	
Cl			−0.40		−0.40	−0.40	

[a] For CASSCF/6, the active space is limited to 6 MOs populated with 6 electrons describing the Cr≡Cr triple bond. [b] For CASSCF/8, the active space includes 8 MOs populated with 8 electrons and accounts for nondynamic correlation in the *xy* plane.

modeled in order to retain a perfect C_{4v} symmetry for the $Cl(CO)_4Cr$ fragment and a C_s symmetry for the complete molecule. All Cr–C_{CO} distances were therefore considered equal (1.959 Å) in the quantum chemical calculations. The Cr≡C distance was taken equal to 1.70 Å. The $Cr(CO)_4$ fragment was assumed to be perfectly square planar. The Cr–Cl and the Cr≡C bonds were taken perpendicular to the $Cr(CO)_4$ plane. One C–H bond of the methyl group was taken in the plane defined by the Cl—Cr≡C—C axis and two opposed carbonyl ligands (eclipsed conformation).

The basis functions for Cr were taken from the DZC basis derived by Tatewaki and Huzinaga.[14] Two GTOs of exponents 0.0726 and 0.0221 were included to describe the 4p shell, and a diffuse d function of exponent 0.0822 was added to the standard set. The inner shells were contracted to a minimum, the 4s and 4p to double-ζ and the 3d to triple-ζ sets, yielding a (12,8,5/5,4,3) basis set for chromium. The basis sets for C, O, and Cl correspond to the MIDI-3 sets of the same authors[15] contracted to split valence, thus giving (7,3/3,2) for first-row atoms and (10,6/4,3) for Cl. Finally, the (4/2) basis set of Huzinaga[16] was used for hydrogen.

In order to provide a correct description of the metal–carbon triple bond, the six MOs representing the Cr–C bonding and antibonding orbitals (σ, π, π^*, and σ^*), altogether populated with six electrons, have been included in the active space of the CASSCF calculations. Consistent CASSCF calculations have been carried out for the $Cl(CO)_4Cr$ fragment of C_{4v} symmetry in its $^4A_2$ quartet state ($\sigma^1\pi^2$) and for the C–CH_3 fragment of C_{3v} symmetry in its quartet ($\sigma^1\pi^2$) and doublet ($\sigma^2\pi^1$) states. All calculations have been carried out with frozen atomic orbitals[17] for the inner shells of Cr (1s to 3p), Cl (1s to 2p), and the first-row atoms (1s).

The theoretical deformation density maps have been computed as the difference between the density distributions generated by the CASSCF molecular wave functions, on the one hand, and the superposition of spherically averaged isolated atoms defined with the same basis sets, on the other hand.

4. Results and Discussion

4.1. Quantum Chemical Description of the Metal–Carbon Triple Bond. The total CASSCF energy for $Cl(CO)_4Cr{\equiv}C{-}CH_3$ is found to be −2024.7824 h. The effect of electron correlation appears quantitatively similar to what had been reported for the model carbyne molecule $Cl(CO)_4Cr{\equiv}CH$.[3] A dissociation energy of 102.4 kcal/mol has been computed for the Cr≡C bond in the methylcarbyne molecule with respect to the superposition of the neutral fragments $Cl(CO)_4Cr$ in its $^4A_2$ ground state (−1947.4435 h) and C–CH_3 in its ^2E ground state (−77.1756 h). The computed dissociation energy is 115.2 kcal/mol if obtained with respect to both fragments computed in the quartet ($\sigma^1\pi^2$) state. These energies are to be compared with the values 107 and 109 kcal/mol, respectively, computed for the dissociation of $Cl(CO)_4Cr{\equiv}CH$ with respect to equivalent fragments in similar states. Even though the present calculations do not account for the opposite effects expected from dynamic correlation and angular flexibility of the basis set, on the one hand, and geometrical optimization of the fragments, on the other hand, the value obtained for the dissociation energy of the triple bond appears plausible. No experimental estimate for the Cr≡C bond energy is presently available, but the energy of the metal–carbon triple bond in $(V{\equiv}CH)^+$, measured in the gas phase to be 115 kcal/mol,[18] provides an interesting point of comparison.

The present study confirms the presence of a negative net charge (−0.32 e) on the carbyne C atom. The order of magnitude of this charge is similar to that of the previous reports.[1-3] Although the net charge on the carbyne C atom appears somewhat diminished with respect to the result of the equivalent calculation carried out for $Cl(CO)_4Cr{\equiv}CH$ (−0.39 e), the polarization of the whole carbyne ligand remains practically unaffected (−0.25 e compared to −0.23 e). All atomic net charges computed for $Cl(CO)_4Cr{\equiv}CH$ and for $Cl(CO)_4Cr{\equiv}CCH_3$ are displayed in Table VII, together with the computed orbital populations of the metal.

It finally appears from the calculations that the presence of the CH_3 substituent does not induce any significant difference between the two metal–carbon π bonds. This point will be discussed in more detail in connection with the density maps.

4.2. Origin of the Cr–C_{CO} Bond Alternation. The theoretical density maps derived from the CASSCF wave functions have been computed in two perpendicular planes each containing the Cl—Cr≡C—C axis (Figure 3b,c). One of these planes (Figure 3b) contains the CH bond assumed to be eclipsed with one carbonyl ligand. The third plane (Figure 3a) contains the metal and the four CO ligands.

One of the puzzling questions about $Cl(CO)_4Cr{\equiv}CCH_3$ is the origin of the Cr–C_{CO} bond length alternation, which reduces the symmetry of the $Cl(CO)_4Cr$ fragment from C_{4v} to C_{2v} ($d_{Cr-C_{1/3}}$ = 1.928 (3) Å, $d_{Cr-C_{2/4}}$ = 1.978 (3) Å, $d_{C_{1/3}-O_{1/3}}$ = 1.128 (4) Å, $d_{C_{2/4}-O_{2/4}}$ = 1.147 (4) Å). A tentative explanation proposed by GK[5] relies on a perturbation caused by the lower symmetry of the CH_3 group. This perturbation either could occur in the isolated molecule or could originate from intermolecular H···Cl interactions.[5b] In either case, it would delocalize over the whole molecule through a hyperconjugative interaction of the methyl group with the chromium atom:

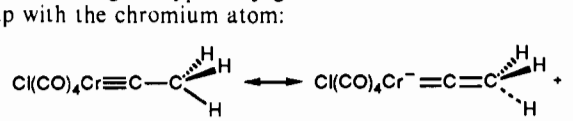

(14) Tatewaki, H.; Huzinaga, S. *J. Chem. Phys.* **1979**, *71*, 4339.
(15) (a) Tatewaki, H.; Huzinaga, S. *J. Comput. Chem.* **1980**, *1*, 205. (b) Sakai, Y.; Tatewaki, H.; Huzinaga, S. *Ibid.* **1981**, *2*, 100.
(16) Huzinaga, S. *J. Chem. Phys.* **1965**, *42*, 1293.
(17) Pettersson, L.; Wahlgren, U. *Chem. Phys.* **1982**, *69*, 185.
(18) Aristov, N.; Armentrout, P. B. *J. Am. Chem. Soc.* **1984**, *106*, 4065.

This hypothesis assumes that a perturbation should affect the electronic structure of the $Cl(CO)_4Cr$ moiety previous to any effective geometrical distortion. In order to check the possibility for an electronic perturbation in the isolated molecule, the CASSCF calculations were carried out by assuming equal $Cr-C_{CO}$ bond lengths, but no symmetry constraint other than C_s was imposed on the wave function.

It finally appears that no detectable difference can be pointed out, neither in the two perpendicular π systems of the Cr≡C triple bond nor in the electronic structure of the four chromium–carbonyl bonds. This practically perfect equivalence of the *xz* and *yz* planes is reflected in the number and in the position of the density contours obtained in the computed map. The zero contour itself, though extremely sensitive to the electronic factors, remains unaffected by a 90° rotation of the molecule, except in the region of the methyl group. The calculations therefore seem to indicate that no delocalized influence of the CH_3 dissymmetry can be traced, even on the C5–C6 bond *in the isolated molecule*.

A similar result is obtained from the unaveraged X–M maps obtained from multipole refinement (Figure 6a), showing a good similarity along the four chromium–carbonyl directions when compared to the spherical model refinement (Figure 5). Furthermore, the three static maps corresponding to the planes respectively defined by C5–C6–H1, C5–C6–H2, and C5–C6–H3 show that the C6–H3 bond, which is quasi-eclipsed with the C3–O3 ligand, does not induce any visible dissymmetry in the distribution of the electron density in the Cr≡C bond. This information, obtained from the experimental distribution, means that the $Cr-C_{CO}$ bond length alternation probably does not originate in a delocalized electronic effect initiated either from intramolecular *or from intermolecular* interactions.

These conclusions are strongly at variance from the interpretation given by GK of their X–X density maps.[5a] Goddard and Krüger reported density peaks consistently higher along the short $Cr-C_{CO}$ bonds (0.5 and 0.8 e Å^{-3}) than along the longer ones (0.4 and 0.4 e Å^{-3}). They interpreted this difference as indicative of a symmetry reduction from 4-fold to 2-fold in the $Cr(CO)_4$ plane. Noticeable differences could also be pointed out between those peaks, opposite with respect to the metal, that are expected to be equivalent.[5] These discrepancies are also obvious in the X–X map of Figure 4a. Since no electronic or structural effect can justify these differences, they should be considered as an artifact originating in the set of measurements.[19] The spherical refinement cannot remedy this defect, but the multipole model acts as a filter for the inconsistencies in the measurement set. As a matter of fact, the unaveraged X–M multipole density map (Figure 6a) provides similar peak heights (0.30–0.35 e Å^{-3}) for all $Cr-C_{CO}$ bonds.

Another argument proposed by GK in favor of a delocalized, hyperconjugative interaction of the methyl group was the high electron density (0.7 e Å^{-3}) obtained along the C5–C6 bond, similar to or higher than the peak heights obtained for the CO bonds and higher than the peak associated with the Cr≡C bonds (0.6 e Å^{-3}).[5] The present work shows however that *the reverse trend is obtained from the multipole refinement*: the respective heights associated with the C5–C6, CO, and Cr≡C5 bonds are 0.3, 0.45, and 0.5 e Å^{-3}. The static (Figure 6) and the dynamic (Figure 8) maps obtained from the multipole model agree with these general directions, in spite of a relative decrease of the Cr≡C peak height. This does not mean however that no hyperconjugative interaction is at work. As a matter of fact, a theoretical deformation density map computed with respect to the $Cl(CO)_4Cr$ and $C-CH_3$ fragments, both in their quartet states (Figure 4), shows that the formation of the triple bond increases the density by about 0.1 e Å^{-3} along the C5–C6 bond, and this additional accumulation extends over the π-bonding regions. This is in agreement with the conclusions obtained from the force field determination of $Br(CO)_4W{\equiv}CCH_3$,[20] of $Cl(CO)_4Cr{\equiv}CCH_3$,[21] and of $Br(CO)_4Cr{\equiv}CCH_3$[22,23] and their partially deuterated derivatives.

It appears from this discussion that both the multipole model maps and the theoretical density arrangement suggest that the distribution of the electron density in the metal complex is equivalent along the four $Cr-C_{CO}$ bonds and remains unaffected by the lower symmetry of the methyl groups. Therefore, we tentatively suggest that the $Cr-C_{CO}$ bond alternation is a local effect of the packing forces.

After the present work had been submitted for publication, Low and Hall (LH) published an article dealing with the same problem and leading to similar conclusions.[24] LH carried out ab initio calculations on $Cl(CO)_4Cr{\equiv}C{-}CH_3$ and optimized the geometry of the molecule at the RHF level. When the 3-fold axis of the methyl group is assumed to be collinear with the Cr≡C axis, the geometry optimization is unable to generate a difference between the two pairs of $Cr-C_{CO}$ bond lengths. However, a 12° tilt of the methyl group axis, originating in intermolecular contacts, is sufficient to generate an alternation of the $Cr-C_{CO}$ bond length very similar to what was experimentally reported.[24]

4.3. Density Maps. The lack of polarization functions in the atomic basis sets used for the derivation of the computed maps somewhat impairs their quantitative accuracy. The influence of the basis set truncation on some specific features of the deformation density are well-known: underestimation of the interatomic accumulation and overestimation of the density buildup corresponding to the lone pairs.[25] These effects can be assessed from a calculation carried out with a large polarized basis set on a molecule with a structure closely related to that of tetracarbonylchloroethylidynechromium, the heterocumulene $(CO)_5Cr{=}N{=}C{=}N{-}(CH_3)_2$.[26] The peaks associated with the C≡O bonds are raised by 0.4 Å. For the other covalent bonds, the increase is ~0.25 e Å^{-3}. On the opposite way, the lone-pair accumulations are decreased by 0.2 e Å^{-3}. Similar effects could be expected from an extension of the Gaussian basis set for the present molecule.

In spite of these quantitative inaccuracies, a remarkable agreement is obtained between the static model maps (Figure 7) and the theoretical ones (Figure 3), except for the oxygen lone pairs of the CO ligands, which do not show up on the model maps. The peak heights associated with the C_{CO} lone pairs and the Cr≡C bond seem to be underestimated with respect to the accumulations associated to CO and C5–C6. This could be related to the existence of a high density gradient along the line connecting the ligand lone pairs to the deeply depopulated $d_{x^2-y^2}$ metal orbitals. Since the density maxima and minima are close to the respective nuclei, a small modification of the scale factor can in this case drastically affect the model distribution.

In spite of an equally high density gradient around the metal atom, density accumulations do appear on the static maps along the bisectors of the *x* and *y* axes, in agreement with the theoretical distribution. The peak height, and the corresponding population of the d_{xy} orbital, appear however somewhat underestimated with respect to the theoretical value. It seems however that the theoretical d_{xy} population is too high due to the neglect of correlation effects in the *xy* plane.

It is interesting to notice, from the chemical viewpoint, that the density pattern both observed and computed for the metal–carbon triple bond is rather similar to the one obtained for the metal–carbonyl bonds. These two metal–ligand interactions are indeed of the same type. The coordination of carbon monoxide

(19) Another possible explanation for these differences could be the correlation between P_{lm}'s and U_{ij}'s. The order of magnitude of the correlation coefficients seems to rule out this possibility.

(20) Nguyen, Quy Dao; Février, H.; Jouan, M.; Fischer, E. O. *Nouv. J. Chim.* **1983**, *7*, 719.
(21) Nguyen Quy Dao; Jouan, M.; Fonseca, G. P.; Tran Huy, N. H.; Fischer, E. O. *J. Organomet. Chem.* **1985**, *287*, 215.
(22) Foulet-Fonseca, G. P.; Jouan, M.; Nguyen Quy Dao; Huy, N. T.; Fischer, E. O. *J. Chim. Phys.* **1990**, *87*, 13.
(23) Foulet-Fonseca, G. P.; Jouan, M.; Nguyen Quy Dao; Fischer, H.; Schmid, J.; Fischer, E. O. *Spectrochim. Acta* **1990**, *46A*, 339.
(24) Low, A. L.; Hall, M. B. *Organometallics* **1990**, *9*, 701.
(25) Smith, V. H. In *Electron Distributions and the Chemical Bond*; Coppens, P., Hall, M. B., Eds.; Plenum: New York, 1982; pp 3–59. See more specifically pp 24–27.
(26) Bénard, M. Unpublished.

is classically described in terms of a σ donation from the ligand and a π back-donation. The orbital interaction diagrams[5a] suggest that the bonding of the carbyne to the metal fragment is by no means different. The dissimilarity is quantitative and comes from the strength of the π back-donation interaction, very close to covalent bonds in the carbyne and leading to a near balance of the populations between overlapping atomic orbitals.[3] The formal electronic configuration for the carbyne would therefore correspond to $\sigma^2\pi^2$. These enhanced π interactions can be correlated with the marked extension of the carbyne density accumulation toward the π-bonding regions: on the observed X–M, static, dynamic, and theoretical maps, the density ellipsoids facing the metal atom and limited by the 0.1 e Å^{-3} contour appear slightly more "flat" for the carbyne than for the carbonyl ligands. The ratio of the major to the minor axes of these ellipsoids is 2.0 for the metal–carbyne bond and 1.6 for the metal–carbonyl bonds on the static model map. These ratios are respectively 2.3 and 1.5 on the theoretical maps. These differences are however at the limit of signification. It can be seen from the theoretical map computed with respect to the superposition of atoms (Figure 3) and, still more explicit, with respect to the superposition of molecular fragments computed in their quartet states (Figure 4) that this accumulation of density, largely extended to the π-bonding regions, originates in part from the depopulation of the carbynic carbon p_x orbitals but mainly comes from the transfer of metal d_{z^2} electrons. Since the resulting density accumulation is polarized toward the C5 atom, this transfer explains the origin and the localization of the negative net charge that theoretical treatments consistently assign to the carbyne carbon.[1-3]

4.4. Chromium d-Orbital Populations. The agreement between the multipole model maps and the theoretical ones is confirmed by the comparison of the chromium d-orbital populations obtained from both distributions (Table VII). The only significant discrepancy between the theoretical and the experimental orbital populations concerns the d_{xy} orbital, which is attributed 33% of the population from the CASSCF calculation and 27% only from the multipole model distribution. This can be traced to the design of the active CASSCF space in the theoretical treatment, which does not account for the nondynamic correlation effects in the xy space. These correlation effects had been specifically studied in a previous work on $Cl(CO)_4Cr{\equiv}CH$ by adding to the CASSCF active space the highest occupied and lowest unoccupied MOs of b_2 symmetry in the C_{4v} point group. These orbitals respectively represent the bonding and antibonding combinations of the metal d_{xy} orbital with the in-plane carbonyl π^* orbitals. This calculation, including eight electrons and eight orbitals in the CASSCF calculations, was referred to as CASSCF-8.[3] Apart from a substantial decrease of the total energy, this account of the metal–CO π correlation has lead to some reorganization of the electron density in the xy plane, reducing the d_{xy} population from 1.74 to 1.59 e (Table VII). This trend is in keeping with the observed d populations.

It can be noticed that the populations of the d orbitals facing the carbyne (d_{z^2}, d_{xz}, d_{yz}) display relatively small deviations from isotropy compared to the population of metal d orbitals facing the carbonyl ligands (Table VII). This trend toward a balance of the populations of the metal and carbon orbitals involved in the Cr≡C triple bond reflects the more homopolar character of the metal–carbyne interactions compared to the metal–carbonyl ones. Finally, it must be reminded that the "d-orbital populations" refined from the multipole model include the minor contributions from the 4s and 4p metal orbitals. The Mulliken population analysis of the CASSCF wave function indicates that the total population of the 4s and 4p shells amounts 0.51 e. The computed net charge of the metal atom is therefore +0.33 e, in excellent—and possibly fortuitous—agreement with the value of 0.40 (8) e obtained from the multipole model refinement.

At variance from this latter result, the net charge distribution derived from the multipole refinement is quite unreliable for C and O atoms, in probable relation with the lack of refinement of the κ' expansion–contraction coefficient. Part of these discrepancies could also originate in the arbitrary character of the space partitioning. Concerning this latter point, the "atomic basins" defined from the topological analysis of the total electron density, either theoretical[27] or experimental,[28] could provide in the near future a domain for charge integration defined upon chemical grounds.

Conclusion

The present study provides the first experimental confirmation of the electron reorganization assessed from quantum chemical calculations to occur in the formation of a metal–carbon triple bond. At variance from the X–X density distributions, the X–M static and dynamic maps obtained by using Hansen and Coppens's multipole refinement technique have provided reliable and significant information. A comparison of the model static maps with a theoretical distribution obtained from CASSCF calculations justifies the interpretation of the Cr≡C bonding in terms of a σ donation and π back-donation with marked trend toward homopolarity for the π bonds. Both the experimental and the theoretical distributions suggest that the observed alternation of the $Cr-C_{CO}$ bond lengths is a local effect due to packing forces. No delocalized electronic influence, either intra- or intermolecular, could be detected. The metal d-orbital populations derived from the multipole analysis of the experimental distribution display near quantitative agreement with those obtained from the Mulliken populations of the CASSCF wave functions.

Acknowledgment. We are very much indebted to Professor C. Krüger for providing us with the set of X-ray diffraction measurements used in the present work as a basis for the multipole model refinement. Quantum chemical calculations have been carried out on the IBM-3090 computer of the Centre de Calcul de Strasbourg, and multipolar refinements have been performed on the IBM-4381 computer of the Centre de Traitement de l'Information de l'Ecole Centrale, Paris. We thank the staff for cooperation.

Supplementary Material Available: Tables S1–S3, listing thermal parameters, interatomic distances, bond angles, and dihedral angles of the methyl group, and Figures S1–S3, showing the X–X spherical density in a plane containing the Cl—Cr≡C—C axis, the residual density maps for the spherical and the multipolar models in the two principal planes, and the static maps for the C6–H2 and C6–H3 bonds (10 pages); a table of calculated and observed structure factors (34 pages). Ordering information is given on any current masthead page.

(27) (a) Bader, R. F. W.; Essén, H. *J. Chem. Phys.* **1984**, *80*, 1943. (b) Bader, R. F. W.; MacDougall, P. J.; Lau, C. D. H. *J. Am. Chem. Soc.* **1984**, *106*, 1594. (c) Bader, R. F. W. *Acc. Chem. Res.* **1985**, *18*, 9.

(28) (a) Bader, R. F. W.; Laidig, K. E. *The Application of Charge Density Research to Chemistry and Drug Design*; NATO ASI Series, in preparation. (b) Stewart, R. F. *Ibid.*